Acta Mechanica Slovaca **28 (3): 74 - 83,** September **2024**
https://doi.org/10.21496/ams.2024.025

Acta Mechanica Slovaca
ISSN 1335-2393
www.actamechanica.sk

Characterization of Nanostructured Magnetic alloy Based on Fe- Nd-Gd-B Produced by Mechanical Synthesis

Rachid Boughedaoui [1], Habib Achache [2], Abdennour El Mohri [3], Rachid Zahi [4,*], Mohamed Azzaz [5]

1 University Yahia Fares of Medea, Algeria
2 University of Oran 2 Mohamed Ben Ahmed, Algeria
3 LMP2M Laboratory, University of Medea, Algeria
4 LPMM Laboratory University of Sidi Bel Abbes, Algeria
5 LSGM Laboratory, USTHB Bab-Ezzouar Algeria

Abstract: This paper examines the effect of Nd substitution by Gd on the exchange coupling in the $Nd_2Fe_{14}B$ nanocomposite. The structural, microstructural, and magnetic properties of Fe76 Nd(16-X) GdXB8 alloy (X = 0, 2, 4, 8, and 16) were investigated. Nanocrystalline alloy samples Fe76 Nd(16-X) GdXB8 (in atomic percentages) were prepared from pure elemental powders by mechano-synthesis. The obtained materials were characterized by X-ray diffraction (XRD), which helped track the dissolution of neodymium and gadolinium in the iron matrix. The maximum crystallite size obtained was 6.5 nm with a microstrain of 1.49% for our powders. Magnetic characterization was performed using a vibrating sample magnetometer (VSM). Results indicate that the optimal Gd concentration for magnetic refrigeration applications is approximately 4%, which provides a balance between superior magnetic coercivity, thermal stability, and nanostructured grain refinement. This finding suggests that the Fe76Nd12Gd4B8 alloy is most suitable for such applications, combining desirable magnetic properties with enhanced microstructural characteristics.

Keywords: Nanostructured material, Rare earth compounds; Characterization; Fe-Nd-Gd-B; powders alloy; structural characterizations, Magnetic characterizations

1. Introduction

The growing demand for Nd-Fe-B-based magnets in the emerging new energy sector is causing a concerning depletion of critical rare earth elements such as neodymium, praseodymium, dysprosium, and terbium, thereby disrupting the global supply structure. To address this situation, gadolinium (Gd), being more abundant and economical, emerges as a promising alternative despite its intrinsically inferior magnetic properties. Studies have demonstrated that the partial substitution of Gd in Nd-Fe-B alloys improves thermal stability, strengthens exchange interactions, and increases coercivity, thereby optimizing magnetic performance. Furthermore, the integration of Gd promotes a better grain structure and optimizes grain boundaries, enhancing the performance of sintered Fe-Nd-B magnets. However, the understanding of the relationships between composition and properties in ternary Gd-Fe-B alloys remains limited. Therefore, our study aims to deepen the analysis of the magnetic properties, microstructure, and phase precipitation of nanocrystalline $Fe_{76}Nd_{16}Gd_xB_8$ alloys. This research is essential to optimize the use of gadolinium in the design of advanced permanent magnets, providing innovative solutions to challenges related to the scarcity of rare earth elements while ensuring superior magnetic performance for various technological applications.

*** Corresponding author:** Rachid Zahi, ***E-mail address:*** *zahirachid72@yahoo.fr*

Numerous studies have driven innovations in magnetocaloric materials and Nd-Fe-B permanent magnets. Kitanovski [1] introduced new ideas for innovative systems aimed at overcoming existing barriers, offering valuable approaches for researchers tackling challenges in magnetocaloric materials. Bouchekara [2] conducted a study on magnetocaloric materials using molecular field theory and the finite difference method (FDM) to simulate the magnetic refrigeration process, yielding useful simulation results. Additionally, the magnetic study of magnetic refrigerators utilizing the finite element method (FEM) was presented with practical and encouraging outcomes.

Hono [3] performed model experiments using thin films of Nd-Fe-B, achieving an intrinsic coercivity of $\mu_0 Hc = 3$ T and enhancing temperature dependence by magnetically isolating approximately 100 nm Nd_2Fe_14B grains. The continuous formation of thin amorphous Nd-rich phases surrounding Nd_2Fe_14B grains is a key microstructural feature of high-coercivity Nd-Fe-B magnets. Woodcock [4] employed a combination of high-resolution characterization, molecular dynamics, and micromagnetic simulations, along with thick film model systems, to gain valuable new insights into the coercivity mechanisms in R-Fe-B magnets.

Yan [5] investigated the effect of gadolinium (Gd) content on the microstructure and magnetic properties of sintered $Nd_{(33.03-x)}$ $Fe_{65.65}$ $Gd_xB_{1.32}$ (x = 0-2) alloys to enhance the thermal stability of Nd-Fe-B and reduce raw material costs. They demonstrated that better magnetic performance could be achieved by adding Gd (0-1.5 wt%) through partial substitution of Nd in $Nd_{(33.03-x)}$ $Fe_{65.65}$ $Gd_xB_{1.32}$.

Sari [6] presented regulations that offer excellent opportunities for the emergence of new magnetic refrigeration technologies. In recent years, magnetic refrigeration has been considered a serious alternative to conventional systems, with the proof of concept already established. The next step is to deploy these systems to society. Sergio [7] synthesized magnetite nanoparticles of various sizes using a solvothermal process, maintaining their stoichiometric composition and unique structural phases. The powder grain size was reduced to less than 1 µm by combining hydrogenation-disproportionation-desorption-recombination, hydrogen decrepitation, and helium jet milling (He-JM).

Coey [8] reviewed the development of permanent magnets, particularly focusing on modern powerful alloys containing rare earths like neodymium and samarium. The powder size was comparable to that of the single domain of Nd_2Fe_14B. Xu [10] studied the substitution of Nd with Gd in Nd-Fe-B magnets, showing that grain size decreases with the addition of Gd. Curie temperatures (Tc) improve with increasing Gd content, indicating enhanced thermal stability of the magnets. However, coercivity and saturation magnetization decrease with higher Gd content due to the low magneto crystalline anisotropy and saturation magnetization of Gd_2Fe_14B.

Ma et al. [11] experimentally investigated the microstructure, crystalline structure, and magnetic properties of $(Nd_{0.7}Pr_{0.1}5RE_{0.1}5)_{2.2}8Fe13.58B1.14$ (RE=La, Ce, Y) alloys prepared by arc melting. Results showed that all alloys annealed at 1173 K for 360 hours contained the isotropic Nd_2Fe_14B phase, with coercivities of 12.3 kOe, 13.2 kOe, and 8.5 kOe, and Curie temperatures of 569 K, 552 K, and 576 K, respectively. Boughedaoui [12] characterized a nanocrystalline alloy Fe76Nd16B8 (atomic %) from pure elemental powders through high-energy mechanical grinding, using techniques like X-ray diffraction (XRD) to dissolve neodymium into the iron phase over milling time. After 20 hours of milling, high-temperature VSM showed that the treated material began to gradually lose its magnetic qualities at T = 80 °C, and above the Curie temperature, the material is considered demagnetized.

Popov [13] presented advancements in 3D printing of permanent magnets, including both rare earth (RE) and non-RE magnets, as well as prospects for electron beam melting (EBM) of MnAl(C). Ozdemir [14] encapsulated hydroxyphenyl acetic acid (3-HPAA) in alginate-chitosan nanoparticles via ionic gelation and characterized these nanoparticles using various techniques. Croat [15] traced the historical evolution of major families of permanent magnets, highlighting the development of the KS Steel magnet in 1917. Liu [16] summarized the principles of non-RE additives and diffusion sources to enhance the magnetic properties of Nd-Fe-B magnets, utilizing Al-Cr coatings to increase coercivity. Kurt [17] discussed future directions for non-RE GBD additives. Sevinç [18] studied the microstructure

and mechanical properties of Cr-Ni steel and Cr-Ni/ZrO_2 nanocomposites, demonstrating the effectiveness of nano-ZrO_2 particles. Zhou [19] analyzed the magnetic properties of Gd-Fe-B alloys, showing stability of hard magnetic properties after annealing. Elkhneny [20] investigated phase transitions in R_2Fe_14B compounds, confirming first-order transitions. Zhang [21] explored a high-entropy amorphous alloy Er20Ho20Gd20Ni20Co20, revealing excellent cryogenic magnetocaloric performance. Saidi [22] examined the effect of substituting iron with chromium in $Gd_2Fe_17\text{-}xCr_x$, observing an increase in the unit cell volume. Finally, Wang [23] reviewed the magnetic properties of rare earth transition metal oxides, proposing new ideas to enhance the magnetocaloric effect and promote low-temperature magnetic refrigeration.

2. Experimental Section

The High-purity elemental powders of Fe (50 µm), Nd (50 µm), Gd (50 µm) and B (20 µm) were employed to synthesize Fe76 Nd(16-X)GdXB8 (X=0, 2, 4, 8, and 16) alloys through high-energy mechanical alloying in a Retsch PM400 planetary ball mill equipped with steel balls (Ø 20 mm). The ball-to-powder weight ratio was maintained at approximately 20/1, and the rotation speed was set to 400 rpm. To mitigate atmospheric contamination, the milled powders were processed under a controlled atmosphere of argon. To prevent overheating during milling, each 15-minute milling interval was followed by a 15-minute milling-free pause.

Scanning electron microscopy (SEM) was employed to monitor morphological changes in the powder particles. The evolution of the phase transformation in the powder mixtures, with a milling duration of 30 hours and X varying from 0 to 16, was investigated by X-ray diffraction (XRD) using a Panalytical X'Pert Pro instrument. The apparatus, equipped with a copper anticathode tube featuring a wavelength (λ) of 1.5406 Å, a linear detector, and a rear monochromator (pixel), operated at an acceleration voltage of 45 kV and an intensity on the anticathode of 40 mA. The chosen angular interval 2Θ ranged from 10° to 140° with a step size of 0.04° and a counting time of 1600s per step. Parameters like lattice parameters and crystallite size were determined using the High Score plus Software based on the Bragg method.

The magnetic properties of the powders were investigated utilizing a vibrating sample magnetometer (VSM, Microsens type EV9) with the application of a magnetic field up to ± 12.5 kOe at both room temperature and elevated temperature. The primary objective of this VSM (Vibrating Sample Magnetometer) is to ascertain, based on the applied magnetic field and temperature, the magnetic properties of the alloy developed through hysteresis cycles.

3. Results and Discussion

3.1. Morphology Evolution

Scanning electron microscopy combined with energy dispersive X-ray spectroscopy (SEM + EDX) highlighted the different morphologies of the powders obtained, and confirmed the conclusions drawn from the analysis of the X-ray diffractograms. The SEM images (Fig.1), obtained with the secondary electron (SE) detector, show the most significant morphological changes at the end of the milling process. The initial Nd powders have coarse prismatic shapes, the iron powders have rounded, almost spherical shapes and the pure gadolinium powders are particles with a spherical or irregular morphology.

The powders are soft, they tend to agglomerate during cold welding and form larger particles during the initial milling phase. Micro forging causes changes in the shape of the individual particles, which are repeatedly impacted by the high kinetic energy milling balls. In the final milling stage (30h) (Fig. 2), a significant refinement and reduction in particle shape is almost uniform and the particle size distribution is narrow.

The various elements (Fe, Nd, Gd and Fe) appear to be 'welded' together, and the particles bear the obvious marks of the multiple breaking and welding events (Figure 2) undergone during the synthesis process. It should be noted that some debris from flatter, more angular particles was present in the ground powders. This debris is mainly produced as a result of the compressive force exerted on the particles by the successive high-energy collisions between the balls and the walls of the jars. In this way, the powder is thrown roughly against the walls and remains stuck there as a result of the violent impacts of the beads and is consequently subjected to successive crushing.

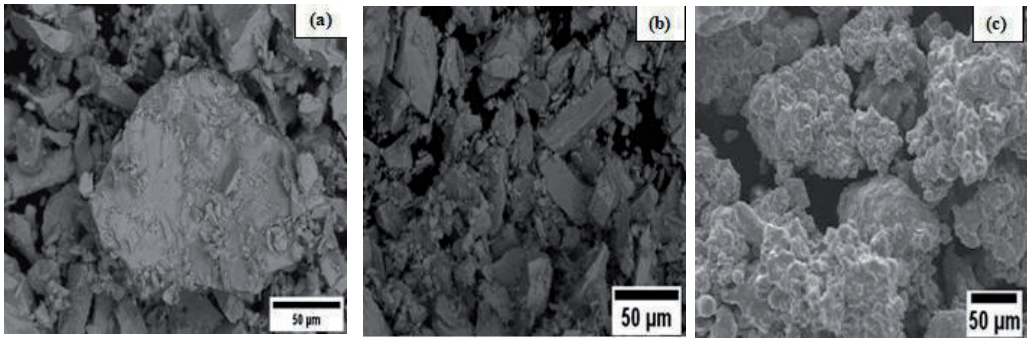

Figure 1: Morphology and SEM images of pure powders. (a) Gadolinium powder morphology. (b) Neodymium powder morphology. (c) Iron powder morphology.

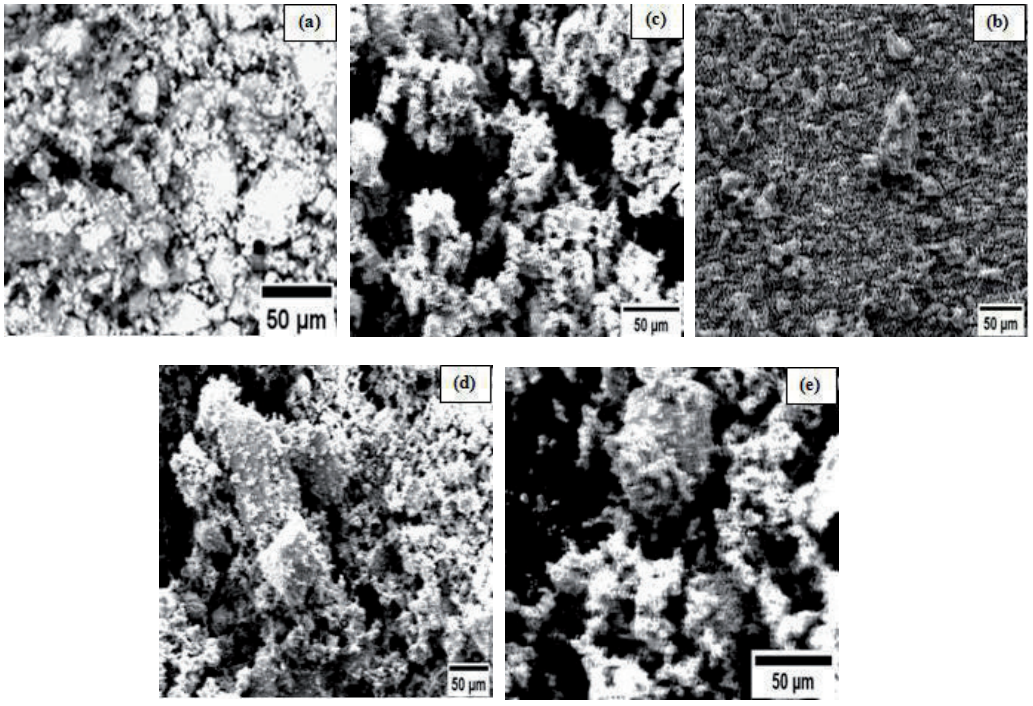

Figure 2: Evolution of the morphology and SEM images of Fe_{76} $Nd_{(16-x)}$ Gdx B_8 alloy powders for x = 0%, 2%, 4%, 8%, and 16% after 30 hours of milling.

3.2. Qualitative analysis

To determine the integrity and elemental concentration of the starting elements in the final mixtures obtained at the end of the mechanical alloying process, elemental mapping by energy dispersive spectrometry (EDS) was developed. The elemental compositions of all the alloys with their EDX spectra are shown in Figures 3 and 4. It can be seen that the distribution of the elements Nd, Gd and Fe is homogeneous, within the error limit of this method, with Boron being minimal and very light not being quantified, indicating that the four elements have completely alloyed and that the solid solution of each starting composition has formed . These results are in good agreement with those obtained by X-ray diffraction.

All the proportions are very close to the desired nominal composition for each alloy. These results confirm that the milling process was carried out under good conditions and that contamination was avoided by choosing a moderate speed to ensure an energy balance between the welding and fracturing phenomena, obtained after studying the physics of mechanical alloys in a planetary ball mill. As a result,

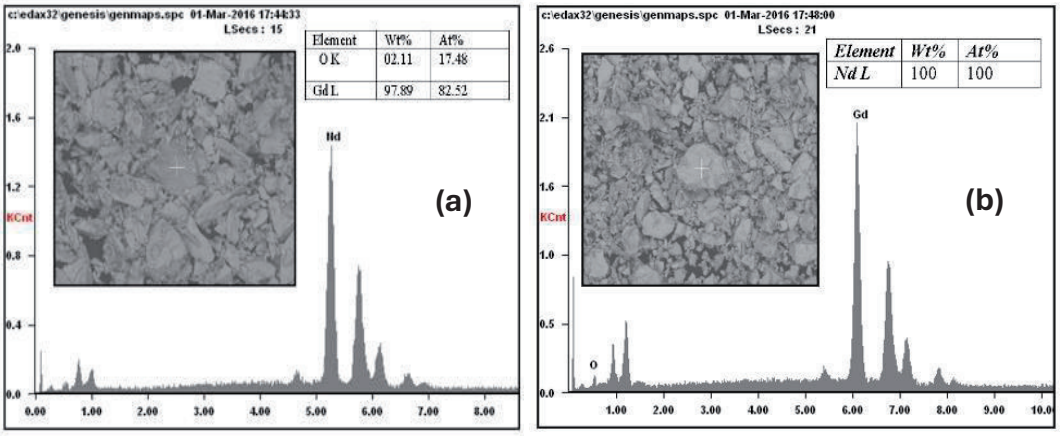

Figure 3: EDX spectra for samples of: (a) pure Gd powder and (b) pure Nd powder

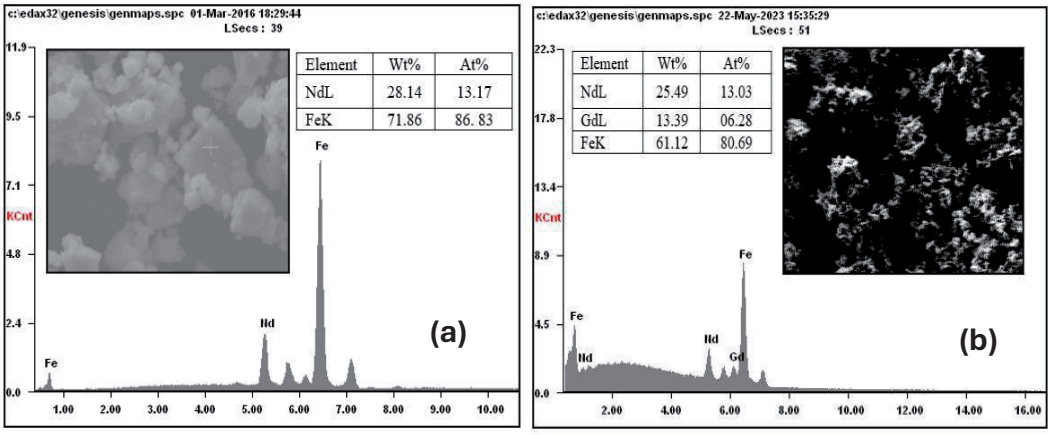

Figure 4: EDX analysis of Fe76 Nd(16-X) GdXB8 alloy powder samples with: (a) X=0 % and (b) X=4%

kinematic calculations show that the moderate milling regime, characterized by a balance between the rotational speed of the jars (ωj) and the rotational speed of the plate (ωp), allows optimum dissolution of the powders and avoids contamination.

3.2. X-ray diffraction pattern and structural changes

The different diffractograms of powders milled for 30 h Fe_{76} $Nd_{(16-X)}Gd_XB_8$ elaborated for different gadolinium contents for (x=0, 2, 4, 8 and 16%). The diffractograms of the pure powder were recorded in the range 10°< 2θ<120° with an angular step of 0.02° to minimise the background noise, and to collect all the information contained in the shape, width and profile of the lines. The X-ray diffraction spectra were simulated using X'Pert High Score software. This software uses analytical functions approximating the Pseudo-Voigt function. It first displays the diffractograms and then adjusts each peak using a Gaussian and Lorentzian skin. Figure 5(a), shows the X-ray diffraction patterns of the powder mixture ($Fe_{76}Nd_{16}B_8$, $Fe_{76}Nd_{14}Gd_2B_8$, $Fe_{76}Nd_{12}Gd_4B_8$, $Fe_{76}Nd_8Gd_8B_8$ and $Fe_{76}Gd_{16}B_8$) after high-energy mechanical milling for a period of 30h, including comparison with the diffractogram of the pure powder.

The spectra of the pure elements reveal the presence of peaks corresponding to the centred cubic (cc) structure of iron (α-Fe), identified by the (110), (200), (211) and (310) planes, as well as that of neodymium (Nd) and gadolinium (Gd) adopting a compact hexagonal (hcp) structure, characterised by the (111), (200), (220), (311), (222), (400), (331), (420) and (422) planes. After 30 hours of milling, we observed the total disappearance of the peaks, with the exception of the (111) plane for neodymium and gadolinium, in all the compositions studied. At

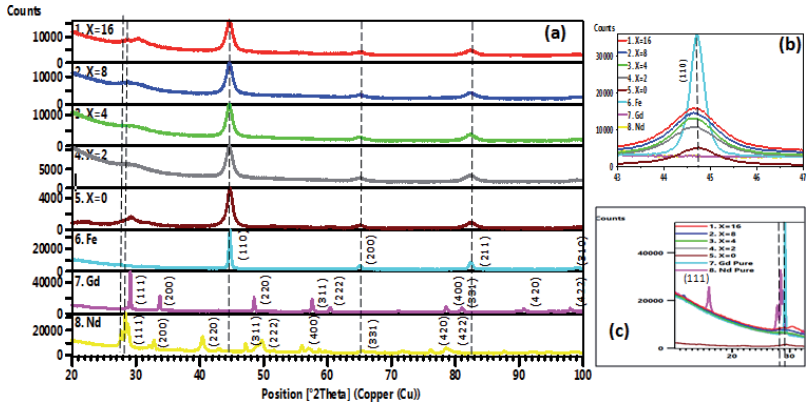

Figure 5: Evolution of the X-ray diffractograms of $Fe_{76}Nd_{(16-X)}$ $GdxB_8$ alloy powder ground for 30h: (a) X-ray diffraction spectra of $Fe_{76}Nd_{(16-X)}$ $GdxB_8$ samples (x=0, 2, 4, 8 and 16), (b) Evolution of the main iron (110) peak according to gadolinium content, (c) Evolution of the neodymium and/or gadolinium peaks (111) as a function of the Gd content.

the same time, the iron peaks became asymmetric and shifted towards the small angles.

This shift, which can be seen in our spectra, confirms the major dissolution of Nd and/or Gd atoms in the centred cubic (cc) structure of iron, leading to the formation of Fe-Nd-B and/or Fe-Gd-B solid solutions. The angular shift of the diffraction peaks in our spectra can also be attributed to first-order internal stresses (microdistortions) induced by milling. In Figures 5(b) and 5(c), we also noted a broadening of the diffraction peaks accompanied by a significant decrease in their intensities. This broadening is attributable to a continuous decrease in crystallite size, associated with an obvious introduction of second-order stresses.

At the level of the main and most intense plane (111) of the compact hexagonal structure (hcp) of Nd and/or Gd, a significant shift of the peaks towards the large angles is attributable to the formation of new solid solutions of iron in the hexagonal structures (hcp) of Nd and/or Gd. There is also a shift of the main neodymium and gadolinium peak towards the small angles. This shift results, on the one hand, from the formation of a solid solution of iron in the neodymium and/or gadolinium and, on the other hand, from the introduction of first-order stresses. These stresses act at the macroscopic level (on a few grains) and alter the mesh parameter (the enlargement of the mesh parameter is envisaged by milling). This phenomenon suggests a structural modification induced by the milling process, highlighting the significant effects of the new solid solutions and stresses on the crystallographic properties of the materials studied. Figure 6 presents the evolution and identification of the phases obtained during the production of Fe_{76} $Nd_{(16-X)}$ $GdxB_8$ nanostructured alloys as a function of different Gd contents.

For the Fe_{76} $Nd_{(16-X)}$ $GdxB_8$ alloy (x=16), Figure 6(d) shows the disappearance of neodymium peaks located at large angles, specifically at $2\theta = 46.94°$, 55.68°, 58.39°, 68.56°, 75.73°, 78.06°, and 87.24°. This disappearance is accompanied by a decrease in intensity and a broadening of the iron peaks.

In Figures 6(a), (b), and (c), we also observe, with the appearance of the most intense neodymium peaks at angles 29.32° and 31.92° for x=0, a reduction in intensity along with a broadening of the peaks. This correlation indicates the insertion of a significant quantity of neodymium atoms into the body-centred cubic α-Fe (bcc) lattice, leading to the formation of a solid solution phase of gadolinium in iron. This phenomenon is also attributed to the insertion of a small quantity of iron atoms into the hexagonal close-packed (hcp) structure of neodymium, resulting in the formation of a second phase.

As can be seen in Fig. 6(b) and 6(c) for the two alloys $Fe_{76}Nd_{12}Gd_4B_8$ and $Fe_{76}Nd_8Gd_8B_8$, the neodymium and gadolinium peaks defined by the (200), (220), (311), (222), (400), (331), (420) and (422) planes disappear. The absence of these peaks is always accompanied by the decrease and broadening of the iron peaks, which corresponds to the insertion of the quantities of Nd and Gd atoms into the dominant Fe(α) (cc) structure, leading to the

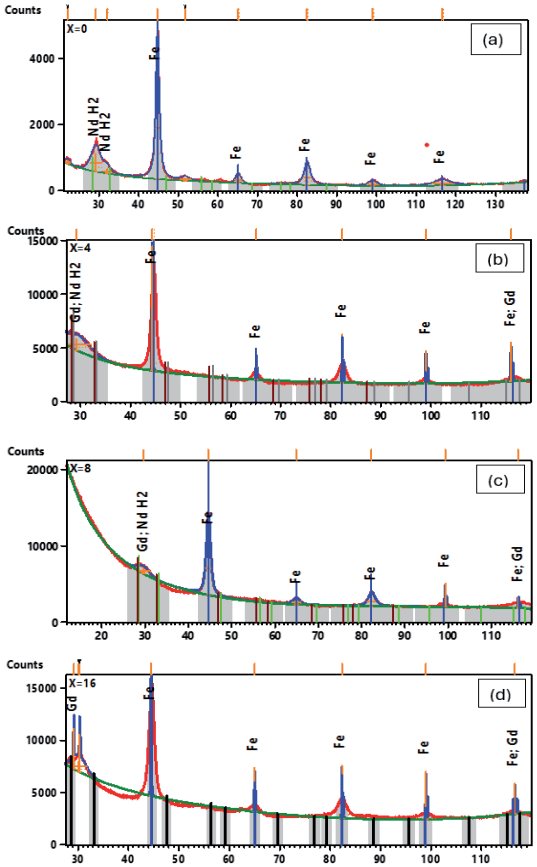

Figure 6: Phase evolution and identification for $Fe_{76}Nd_{(16-X)}GdxB_8$ powder alloys milled for 30h. a) X=0%, b) X=4%, c) X=8% and d) X=16% by mass.

formation of the main Fe(Nd), Fe(Gd) and Fe(Nd, Gd) solid solution phase. On the other hand, we notice the appearance of a peak at about 2θ = 29.7° for the $Fe_{76}Nd_{12}Gd_4B_8$ alloy with x=4% in Fig. 6 (b) and 2θ = 30.14° for the $Fe_{76}Nd_8Gd_8B_8$ alloy with x=8% Fig. 6 (c). This appearance of these peaks close to the (111) plane and shifted towards the large angles in the aforementioned alloys corresponds to the insertion of iron atoms into neodymium and gadolinium, leading to the formation of two compact hexagonal phases (hcp). These phases were quantified using X' Pert High Score software, showing rates of 88% Fe(dc), 6% Nd(dcp) and 6% Gd(dcp) for the $Fe_{76}Nd_{12}Gd_4B_8$ alloy, and rates of 87% Fe(dc), 6% Nd(dcp) and 6% Gd(dcp) for the $Fe_{76}Nd_8Gd_8B_8$ alloy.

In the same context for the $Fe_{76}Gd_{16}B_8$ alloy for x = 16%, Fig. 6 (d) shows us the appearance of two phases, one dominant is represented by the structure (cc) of the solid solution of gadolinium in iron (cc), the other minor phase of compact hexagonal structure , determined by the solubility of iron atoms in gadolinium quantify using software used X' Pert High Score indicating a rate of the phase of 90% iron Fe(α)(cc) and 10% gadolinium Gd (hcp).

For the calculation of the lattice parameter of $Fe_{76}Nd_{(16-X)}GdxB_8$ powders obtained after 30h milling for different Gadolinium content, we considered the most intense peak (110) of Fe(Nd, Gd, B) iron and α-phase before and after solid solution formation respectively.

The evolution of the lattice parameter for nanostructured $Fe_{76}Nd_{(16-x)}GdxB_8$ alloys for 30h of milling as a function of the Gd content is shown in Figure 7.

We observed a slight increase in the lattice parameter as a function of the Gd content (X=0 to X=16). Indeed, its value increases from 0.28613 nm for $Fe_{76}Nd_{(16-x)}GdxB_8$ with X=0%, to 0.28691 nm for X=16%. The variation in the lattice parameter is due to the difference between the atomic radii of iron and those of Nd and Gd, which are 0.140 nm, 0.185 nm, and 0.180 nm, respectively. The evolution of the lattice parameter a (nm), as reflected in our diffractograms by a shift in the diffraction peaks toward smaller angles, is due to the large atomic radius of Nd (Atomic radius of Nd = 0.185 nm) and Gd (Atomic radius of Gd = 0.180 nm) compared to that of Fe (Atomic radius of Fe = 0.140 nm). In general, the increase in the lattice parameter is attributed to the formation of the solid solution that precedes the formation of the amorphous phase. For the maximum lattice parameter value of 0.287523 nm of the $Fe_{76}Nd_{12}Gd_4B_8$ alloy, the lattice parameter value is closest to that of bulk pure iron, which is 0.2860 nm.

Figure 8 shows the evolution of the average grain size, <D (nm)>, and the average value of microdistortions, as a function of the percentage of Gadolinium Gd. We noticed that the average grain size decreases monotonically with increasing Gd percentage (from x=0 to x=16%). This decrease in <D> is accompanied by an increase in the rate of microdistortions with the rate of Gd (X=0 to X=16 %). Indeed, the average grain size decreases from 8.8 nm (for x=0%) down to 5.6 nm (for x=16%) while the microdistortion rate increases from 1.14% (for X=0%) up to 1.79% (for X=16%).

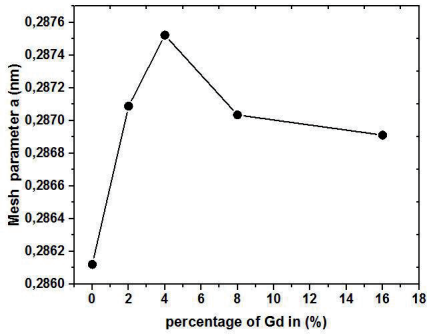

Figure 7: Mesh parameters as a function of Gd content in % (0, 2, 4, 8 and 16%)

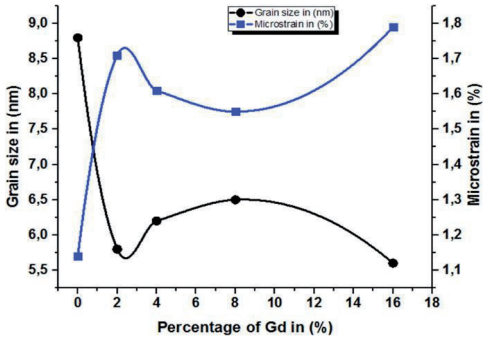

Figure 8: Average grain size and microstrain as a function of Gd content (0, 2, 4, 8, and 16%)

3.3. Magnetic characterization

Before commencing data collection of the milled mixture, M–H curves (Fig. 9, Fig 10) were recorded using a Microsense Vibrating Sample Magnetometer (VSM), Model EZ9, at room temperature. A thorough analysis of the VSM results, illustrated in Figure 11, indicates that the nanostructured Fe-Nd-Gd-B alloy retains its magnetic properties during mechanical milling. Additionally, the maximum coercive field value obtained for x = 4 % Gd is 16.1 kOe after thirty hours of milling, after which it gradually decreases to a minimum value of 14.42 kOe for x = 8 % Gd. For x = 16 % Gd and 0 % Nd, the $Fe_{76}Gd_{16}B_8$ alloy exhibits a coercivity of 15.4 kOe.

Magnetic characterization. Analysis of Fe-Nd-Gd-B alloy powder by VSM gives results in the form of curves called hysteresis loop (fig 9). The variation in magnetic properties as a function of the percentage of Gd for a given milling time can be seen in the hysteresis cycle diagram

The variation of the coercive magnetic field Hc is plotted as a function of the percentage of Gd and Nd with a milling duration of 30 hours, as well as the remanent magnetization Mr and the saturation Ms (figure 11a, 11b and 11c).

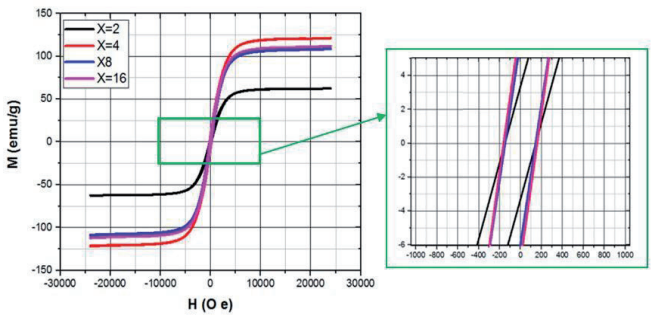

Figure 9: Hysteresis curves (magnetization as a function of applied field) for $Fe_{76}Nd_{(16-x)}GdxB_8$ nanostructured powders (x= 2, 4, 8, and 16)

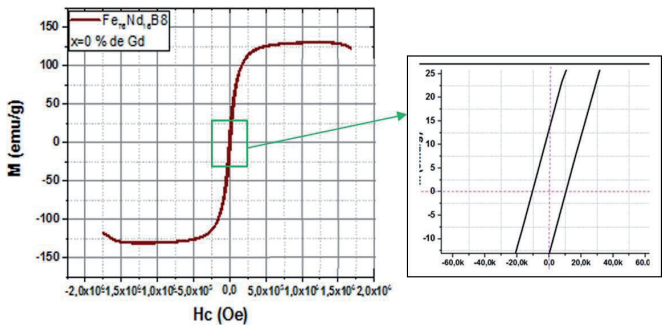

Figure 10: Hysteresis curves (magnetization as a function of applied field) for $Fe_{76}Nd_{(16-x)}GdxB_8$ nanostructured powders (x= 0 % of Gd)

Figure 11a shows the evolution of the magnetic field required to cancel the magnetization of the $Fe_{76}Nd_{(16-X)}Gd_XB_8$ alloy as a function of the percentage X of Gd. Hc does not appear to vary linearly with the percentage of Gd, although there are significant variations. It can be seen that for X= 4% Gd the value of Hc passes through a Maximum value of 16.1 kOe, then the value of Hc decreases to 14.42 kOe which corresponds to the lowest value which is understandable given that there is no longer any Nd and the alloy becomes $Fe_{76}Gd_{16}B_8$.

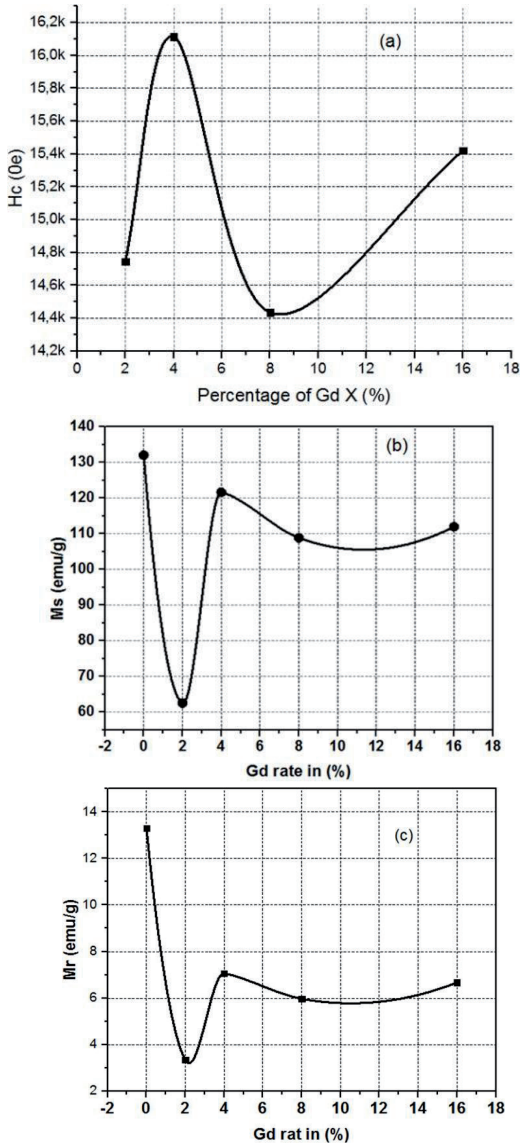

Figure11: Plots of Hc (a), Ms(b) and Mr (c) as a function of Gadolinium percentage X

Regarding saturation magnetization (Ms), its minimum value is observed at x = 2 % Gd, followed by an increasing trend similar to that of the coercive field, reaching 121 emu/g, and then begins to decrease until it reaches 110 emu/g. The remanent magnetization (Mr) shows a minimum value of 3.3 emu/g at x = 2 % Gd, followed by an increasing trend reaching 7.1 emu/g before decreasing to 6 emu/g.

The variation in coercivity (Hc) is associated with various factors such as magnetic domain motion, exchange interactions, magnetic anisotropy, demagnetization effects, surface conditions, and material structure. These factors are influenced by microstrain, grain size, dislocation densities, grain boundaries of crystalline alloys, and residual stresses.

4.Conclusion

The In this study, we investigated the structural characteristics, microstructure, and magnetic properties at room temperature of the nanostructured $Fe_{76}Nd_{(16-X)}Gd_XB_8$ alloy (x = 2, 4, 8, and 16), prepared through high-energy ball milling (mechanical alloying). At the end of the milling process, homogeneous mixtures consisting of very fine particles, with a maximum size of less than 50 µm, were produced. The mixture was primarily composed of nearly round agglomerated grains, along with a few irregularly shaped particles.

Our findings indicate the following:

– *The average grain size decreased progressively as the Gd content increased, which was accompanied by an increase in microstrain.*

– *The average grain size decreased from 8.8 nm to 5.6 nm, while the microstrain rate increased from 1.14% (for x = 0%) to 1.79% (for x = 16%).*

– *In terms of magnetic properties, the magnetic coercivity (Hc) reached a maximum of 1.72 T for 4% Gd and gradually decreased to 1.6 T for 16% Gd.*

For magnetic refrigeration applications, the optimal Gd concentration appears to be around 4%. At this concentration, the $Fe_{76}Nd_{12}Gd_4B_8$ alloy exhibited the best magnetic coercivity and a favourable microstructure while maintaining structural stability. These results suggest that the alloy with 4% Gd is most suitable for applications requiring optimal magnetocaloric effects, thanks to its superior magnetic properties and nanometric grain size. A higher Gd concentration, although accompanied by a further reduction in grain size, seems to lead to a slight decrease in magnetic

performance, making it less effective for refrigeration systems.

This conclusion emphasizes the importance of controlling Gd concentration to optimize the efficiency of alloys for magnetic refrigeration applications, while balancing magnetic and structural properties.

References

1. Kitanovski, A.a.E., P.W, Innovative ideas for future research on magnetocaloric technologies. International journal of refrigeration, 2010. 33(3): p. 449-464.
2. Bouchekara, R.H. and Nahas, M. (2012), Trends in Electromagnetism-From Fundamentals to Applications, IntechOpen, London, SW7 2QJ, UNITED KINGDOM,
3. Hono, K. and Sepehri-Amin, H. (2012), "Strategy for high-coercivity Nd–Fe–B magnets". Scripta Materialia, 67(6): p. 530-535.
4. Woodcock, T.G., Zhang, Y., Hrkac, G., Ciuta, G., Dempsey, N.M. , Schrefl, T. , Gutfleisch, O.and Givord, D. (2012), "Understanding the microstructure and coercivity of high performance NdFeB-based magnets". Scripta Materialia, 67(6), 536-541.
5. Yan.,W., Yan, Sh., Yu, D., Li, K., Li, H., Luo, Y. and Yang, H. (2012), "Influence of gadolinium on microstructure and magnetic properties of sintered NdGdFeB magnets". Journal of Rare Earths, 30(2), 133-136.
6. Sari, O. and Balli,M. (2014),"From conventional to magnetic refrigerator technology". International journal of refrigeration, 37, 8-15.
7. Coey, J.M.D. (1995), "Rare-earth magnets". Endeavour, 19(4), 146-151.
8. Sergio, I., Madrid1, U., Pal, U. and Jesús, F.S.-D. (2015), "Controlling size and magnetic properties of Fe3O4 clusters in solvothermal process". Advances in Nano Research, 2(4), 187- 198.
9. Satoshi, S., Michihide, N., Masashi, M., Yasuhiro, U., Hirokazu, K. and Masato, S., (2015), "Enhancement of Coercivity of Nd-Fe-B Ultrafine Powders Comparable with Single-Domain Size by the Grain Boundary Diffusion Process". IEEE Transactions on Magnetics, 51(11), 2434889.
10. Xu, X.L., Cheng, G., Du, Y.S. and Li, L. (2017), "The Effects of Substitution of Nd by Gd on the Magnetic Properties of Melt-Spun Nd-Fe-B". Advanced Materials Research, 1142, 53-56.
11. Ma, J., Wang, J., Rong, M.H., Rao, G. H. and Zhou, H.Y. (2017), "Microstructure and Magnetic Properties of (Nd0.7Pr0.15 RE0.15) 2.28 Fe13.58 B1.14 (RE=La, Ce, Y) Alloys". Advanced Materials Research, 1142, 57-61.
12. Boughedaoui. R.,Azzaz, M.C., Melouah, M.T., El Mohri, A., Zergoug, M., Lounis, A. and Azzaz, M.(2018), "Structure, microstructure and magnetic properties of nanostructured alloys Fe-Nd-B prepared by mechanical alloying". Journal of Nano Research, 55, 11-21.
13. Popov, V., Koptyug, A., Radulov, I., Maccari, F. and Muller, G. (2018), "Prospects of additive manufacturing of rare-earth and non-rare-earth permanent magnets". Procedia Manufacturing, 21, 100-108.
14. Ozdemir, O.O. and Soyer, F. (2021), "Synthesis, characterization, and antimicrobial activities of 3-HPAA-Alg-Chi nanoparticles". Advances in Nano Research, 11(3), 227-237.
15. Croat, J.J. and Ormerod,J.(2022),"Chapter 1 - The history of permanent magnets.Modern Permanent Magnets, 1-30.
16. Liu, Z., He, J., Zhou, Q., Huang, Y. and Jiang, Q.(2022), "Development of non-rare earth grain boundary modification techniques for Nd-Fe-B permanent magnets". Journal of Materials Science & Technology"98, 51-61.
17. Kurt, A., Helvacıoğlu, H. and Yonar, T. (2022), "Electrochemical treatment of cefalexin with Sb- doped SnO2 anode: Anode characterization and parameter effects". Advances in Nano Research, 13(6), 513-525.
18. Sevinç, Ö. and Diler, E.A. (2022), "Microstructure characterization and mechanical properties of Cr-Ni/ZrO2 nanocomposites". Advances in Nano Research, 13(4), 313-323.
19. Zhou, B., Fan, W., Liao, X., He, J. and Liu, Zh. (2022), "Magnetic properties and phase constitution of rapidly quenched nanocrystalline Gd-Fe-B alloys with various Gd contents". Materials Letters, 317, 132130.
20. Elkhneny, R.M., Aly, S.H., Yehia, S. and Khedr, D.M. (2022), "Magnetic properties and magnetocaloric effect of R2Fe14B compounds with R = Y, Pr, Nd, Sm, Gd, Tb, Dy, Ho and High-Magnetic field phase transitions in the compounds with R = Gd, Dy". Cryogenics, 127: 103567.
21. Zhang, Y., Zhu, J., Li, Sh., Wang, J. and Ren, Z. (2022), "Achievement of giant cryogenic refrigerant capacity in quinary rare-earths based high-entropy amorphous alloy". Journal of Materials Science & Technology, 102, 66-71.
22. Saidi, M., Jaballah, H., Bessais, L. and Jemmali, M.(2023),"Structural, magnetic and magnetocaloric properties of the Gd2Fe17-xCrx (x = 0, 0.5, 1 and 1.5) compounds". Journal of Physics and Chemistry of Solids, 183,111534.
23. Wang, Q., Wu, Q., Cheng, H., Li, X., Yu, N., Pan, M., Yu, Y., Fang, J., Hu, X., Ge, H. and Yang, H. (2023), "Review of the research on oxides in low-temperature magnetic refrigeration". Journal of the European Ceramic Society, 43(15), 6665-6680.